Journal of Applied Geophysics 238 (2025) 105709

Contents lists available at ScienceDirect

Journal of Applied Geophysics

journal homepage: www.elsevier.com/locate/jappgeo

Vector magnetometry to analyse the Caldereta volcano in the canary islands as a possible terrestrial analogue of mars

Marina Díaz Michelena [a,*], Emma Losantos [a], Miguel Ángel Rivero [a], Joana Oliveira [a,b], Óscar García Monasterio [a], Federico Mansilla [c], Ángel Melguizo [a], José Luis García Bueno [d], David Salamanca [a], Sergio Fernández Romero [a]

[a] Space Magnetism Area, Earth Observation and Space Sciences Department, INTA, Torrejón de Ardoz, 28850 Madrid, Spain
[b] Now at Telespazio UK S.L. for the European Space Agency (ESA), European Space Astronomy Centre (ESAC), Camino Bajo del Castillo s/n, Villanueva de la Cañada, 28692, Madrid, Spain
[c] Centro de Astrobiología (CAB), INTA-CSIC, Torrejón de Ardoz, 28850 Madrid, Spain
[d] Quality Department, INTA, Torrejón de Ardoz, 28850 Madrid, Spain

ARTICLE INFO

Keywords:
Magnetometry
Mars
Planetary magnetism
Crustal magnetism
Mars hydromagmatism
Planetary science
Space magnetometers

ABSTRACT

Volcanoes are typical features of terrestrial planets' surfaces. Among the different geological processes which give rise to volcanoes, hydromagmatic eruptions are of particular importance for the search of extraterrestrial life since they require the presence of water.

Phreatomagmatic eruptions on Mars shall resemble those of the Earth. The possibility to perform magnetic surveys on Mars with magnetometers carried by helicopters opens a new scenario to gain more insights on such features. As a natural first step, gathering a database of terrestrial analogue magnetic signatures is desired, prior to magnetic surveys on the Martian surface. In this work we have selected the Caldereta volcano, a phreatomagmatic edifice in Lanzarote Island (Canary Islands), to perform a magnetic survey using on board drones magnetometry. The acquired data will allow to compare future measurements from other similar structures of the "Red Planet". The survey casts vector magnetic field data generated by the volcanic edifice. Additionally, we suggest a simplified structure that mimics the geomorphology observed, we attribute a magnetization to such structure and develop a mathematical model that computes its sourced magnetic field. Finally, we develop synthetic models of a volcano on Mars which have been preliminarily classified as hydromagmatic taking Caldereta simulated structure as a reference.

1. Introduction

The study of hydromagmatism is relevant for habitability studies and life search on other planets given that, on Earth, this phenomenon is a result of magma-water interaction (Mateo et al., 2019). Specifically, hydromagmatism is the phenomenon that occurs when water is involved in a volcanic eruption and therefore requires three main components: a relatively fluid magma, an external input of water and the wall rocks (White and Houghton, 2000). The principle behind it is the rapid heat exchange from magma to the water introduced in the plumbing system of a volcano. This causes its vaporization and leads to rapid steam expansion and pressure build-up in the system, producing fragmentation of the wall rocks and eventually an explosion (e.g. Basaltic Volcanism Study Project, 1981, p. 729; Lorenz, 1986). Hydrovolcanism occurs on Earth in all volcanic settings and is likely to have been common in Mars too, as Mars has widespread volcanism and it is now accepted that water and/or ice is present in its surface and subsurface (e.g. Baker, 2001; Smith et al., 2009). Therefore, it is of special interest to be able to distinguish hydromagmatic edifices on the surface of a planet such as Mars.

Some volcanoes on Mars have indeed been classified as hydromagmatic based on remote sensing data, geomorphological analyses and other considerations (Brož and Hauber, 2013; Brož et al., 2020; Keszthelyi et al., 2010). The confirmation of such hypothesis, though, will require in situ surveys as well as the generation of a database of analogous features on Earth, which can be used as reference.

Magnetometry and gravimetric surveys (or a combination of both) are powerful geophysical tools to delimit geological structures of

* Corresponding author.
E-mail address: diazma@inta.es (M. Díaz Michelena).

https://doi.org/10.1016/j.jappgeo.2025.105709
Received 28 November 2024; Received in revised form 12 March 2025; Accepted 31 March 2025
Available online 7 April 2025
0926-9851/© 2025 The Authors. Published by Elsevier B.V. This is an open access article under the CC BY-NC license (http://creativecommons.org/licenses/by-nc/4.0/).

different magnetic susceptibility or remanent magnetization and density because they yield a contrast of magnetic and gravity values respect to the surroundings. Magnetic surveys are appropriate for those planets which have a global magnetizing field or had one in the past. Surveys made by Mars Global Surveryor (MGS) and Mars Atmosphere and Volatile EvolutioN (MAVEN) spacecraft orbiting Mars and related studies have shown that Mars surface presents a magnetic contrasts (Mittelholz et al., 2018; Langlais et al., 2019; Gao et al., 2021). These features are believed to be the result of magnetized rocks from the Martian crust. New crust is formed by magmatic processes that bring mantle derived melts to the surface where they solidify at a speed that depends on the thermal isolation of the atmosphere, which can play an important factor in the magnetization recorded in such processes in different planetary bodies (Spohn, 2011). This fact, together with an age estimation of distinct features on the surface of the Planet, unveiled that Mars held in early stages, between 4300 and 4200 Ma (Lillis et al., 2013), a global field generated by a core dynamo (Arkani-Hamed, 2005). The lack of magnetic anomalies associated to several basins dated 3900 Ma, lead to set an ulterior limit to the period of activity of the global field (Sandu and Kiefer, 2012). More recently, a study on the magnetic signature associated to Lucus Planum, formed ~3700 Ma ago (Mittelholz et al., 2020), reopened the debate on the time-period there was a global magnetic field on Mars.

The spatial resolution of the magnetic maps is inversely proportional to the distance at which measurements are registered. Therefore, available measurements taken by MGS (1999–2006) and MAVEN (2013 – present) orbiters at altitudes in the order of 400 km and 135 km, respectively provide anomaly maps of limited spatial resolution in the order of 150 km wavelength (Mittelholz et al., 2018; Langlais et al., 2019; Gao et al., 2021). Unfortunately, rovers are not suitable vehicles for this type of survey because: 1) they cover linear distances restricted to tens of km (< 50 km to date; mars.nasa.gov/resources/6471/driving-distances-on-mars-and-the-moon); and 2) they face difficulties to define routes that cross geological interfaces which typically implies rough terrain or even fractures. Therefore, flights closer to the surface with distances less than few tens of meters would provide measurements to build maps of better resolution that in turn would help correlating the magnetic anomalies to different geological features, as done on Earth.

Recently, a first close flight was achieved on the Martian surface by the helicopter Ingenuity (NASA, 2019). This is indicative of the capability of having helicopters / drones carrying magnetometers on Mars in the near future (Mittelholz et al., 2023). Therefore, preliminary studies such as magnetic surveys on well-known terrestrial analogs, must be carried to support the interpretation of future Martian high-resolution close survey data (Díaz Michelena et al., 2022).

With the rapid improvement of multicopter drones, magnetometry on board drones has experienced a notable increase in popularity (Zheng et al., 2021; Tada et al., 2021). Magnetometry on board such drones, compared to ground magnetometry, permits the execution of ordered surveys with denser grids with a relatively low-resolution loss since, depending on the terrain, the flights can be performed at low height (few meters).

As a first step for the univocal identification of hydrovolcanoes on Mars it is necessary to first study analogous features on Earth. In this work we have performed a comparative study of two volcanic features of akin origin and morphology: C27 volcano, on Nephentes / Amenthes Region (NAR), on Mars; and Caldereta volcano in Lanzarote on Earth (Figs. 1 and 2).

2. Geological context

2.1. C27 volcano in Nephentes/Amenthes region

The C27 crater lies within a large field of pitted cones, encompassed between Amenthes Cavi region to the north and Nephentes Planum to the south (10°N to 20°N and 95°E to 125°E, Fig. 1) (Brož and Hauber, 2013), in what here we will call Nephentes/Amenthes Region (NAR). This region can be found close to the dichotomy and is surrounded by two basins of big entity. Utopia, to the north, was likely formed by a giant impact between 4.5 and 4.1 Ga (McGill, 1989; Skinner Jr et al., 2005; Carr and Head III, 2010), whereas Isidis Planitia, to the west, is a

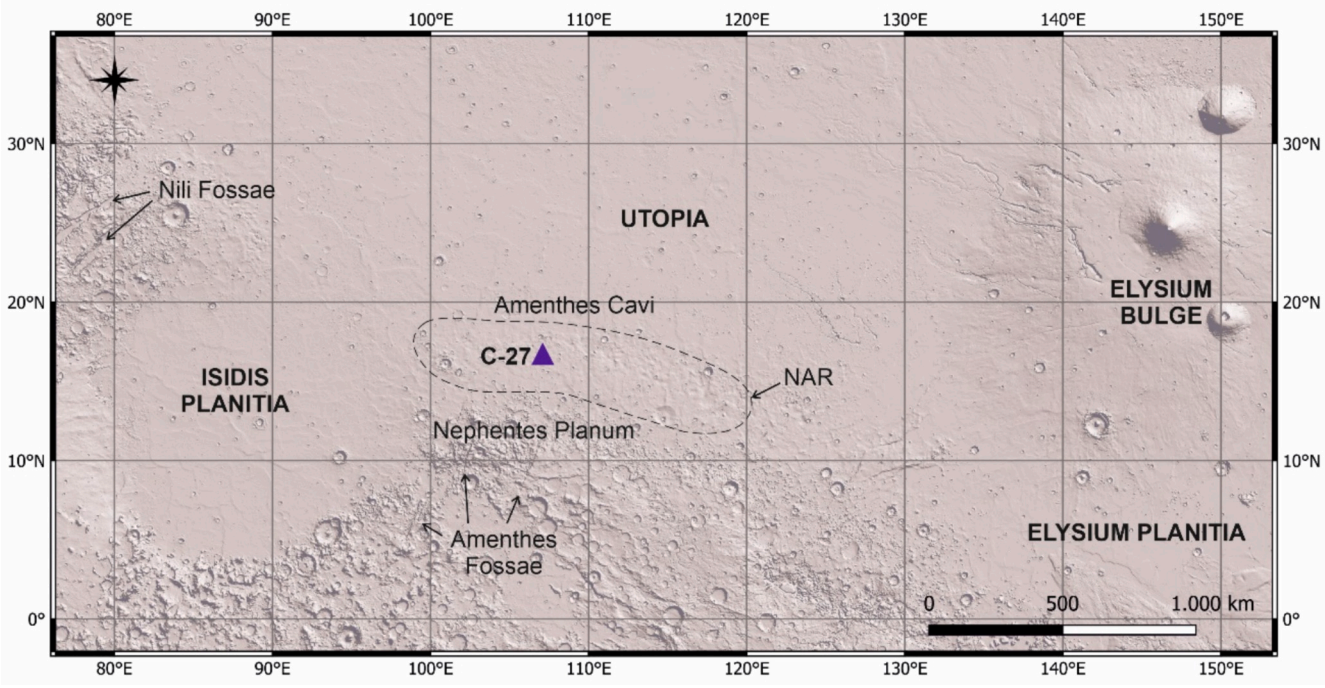


Fig. 1. Location of C27 crater (purple triangle) within the NAR pitted cones area and its regional context in Mars. Map developed from the Digital Elevation Model (DEM) based on data from the Mars Orbiter Laser Altimeter (MOLA; Smith et al., 2001), an instrument on NASA's Mars Global Surveyor (MGS) spacecraft (Albee et al., 2001). Pixel resolution 463 m. (For interpretation of the references to colour in this figure legend, the reader is referred to the web version of this article.)

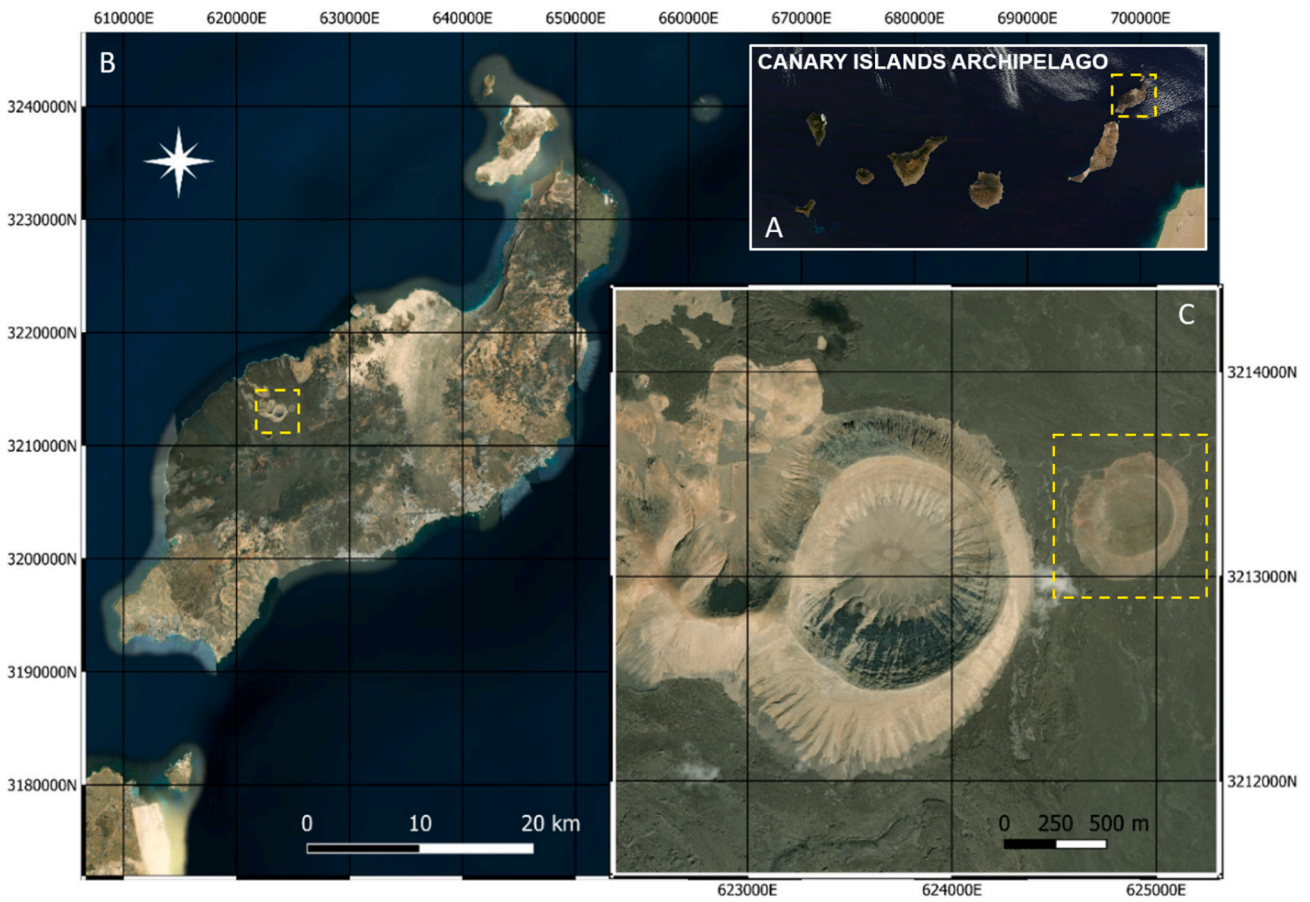


Fig. 2. A. Location of Lanzarote island within the Canary Islands Archipelago; B. Location of Caldera Blanca – Caldereta volcanic complex in Lanzarote Island; C. Satellite image of -Caldereta (the smaller edifice to the east) in the Caldera Blanca – Caldereta volcanic complex. ESRI satellite images.

latter impact (Skinner Jr et al., 2005) that caused the formation of NNE tectonic grabens around it: Nili Fossae to its west and Amenthes Fossae to its east (Erkeling et al., 2011), this later one lying close to the southern end of the NAR. The east of NAR is framed by the Elysium bulge and Elysium Planitia, which are important volcanic centers (Malin, 1977; Plescia, 1990).

The pitted cones of the NAR were originally described as "volcano like forms" by Erkeling et al. (2011) and as mud volcanoes by Skinner Jr and Tanaka (2007) on the basis of their morphological analysis of several landforms. But more recently, Brož and Hauber (2013) suggested a hydromagmatic origin based on their comparative geomorphological study and regional evidences of both subsurface water and volcanic activity around NAR.

2.2. *Caldereta volcano in Lanzarote*

Sitting on the easternmost sector of the Canarian archipelago (Fig. 2A), at approximately 125 km off the African coast and parallel to it, the island of Lanzarote (Fig. 2B) has an abundance of phreato-magmatic vents. This is probably due to the low topography (<300 m above sea level) of the island that favors the entry of sea water into the volcanic systems.

The edifices of Caldera Blanca and Caldereta (West and East edifices respectively in Fig. 2C) are two good examples of them. They both follow a NE-SW alignment of eight volcanic centers, four of them hydromagmatic (García Cacho and Romero, 2000), grouped for their similar volcanological characteristics and their stratigraphical position in relation with other nearby eruptions (Barrera Morate and García, 2011).

This lineation, with an age of less than 2 Ma (Abdel-Monen et al., 1971), likely represents the coastal shoreline previous to the quaternary eruptions (Barrera Morate and García, 2011). They are emplaced in an area that has an average slope of >5 % tilt and is unevenly surrounded by the Quaternary Timanfaya lava flows, which thickness varies around the edifices hampering the identification of the original topography. Caldera Blanca and Caldereta (Fig. 2C) are also considered as one of the best examples of "Islote", in the local terminology, or "kipuka" in the Anglo-Saxon terminology, in the Canary islands since they are a portion of terrain completely surrounded and isolated by the posterior emplacement of lava flows, in this case from the Timanfaya 1730 and 1736 eruption (Galindo et al., 2019).

Caldera Blanca (Fig. 2) is nowadays the largest monogenetic edifice of the archipelago, with a base diameter of 1.7 Km and a 1.1 km crater (Barrera Morate and García, 2011; García Cacho and Romero, 2000), and shows the morphometrical features of a tuff cone (Carracedo and Day, 2002; Romero et al., 2007; Kervyn et al., 2012; Brož and Hauber, 2013; Table 1). It presents outer slopes of ~33° and the inner slopes are not controlled by avalanching of cohesionless granular material. In fact, subvertical slopes are present, probably sustained by indurated tuff material, which yields an exceptionally high crater to cone diameter W_{Cr}/W_{Co} (=0.71) that has been ascribed to phreatomagmatic cypressoid tephra jets or base surges from a funnel-shaped crater cutting into the substrate rocks (Kervyn et al., 2012). This edifice is believed to have being active less than 2 Ma ago (Romero et al., 2007) with strombolian and hydromagmatic activity phases. During its period of activity it emitted some basaltic flows, which were later almost covered by the Timanfaya eruption, as well as alternating ash and lapilli materials of different thicknesses that transition to planar lamination with occasional

Table 1
Summary of the main parameters resulting from the morphometric analysis. Values calculated in previous works have been reproduced as reference. The different acronyms correspond to: σ = error in the units of the magnitude, H = height, W = width, subscript Co = Cone, subscript Cr = Crater; D = crater depth.

Cone (Source)	Type	Base Elevation (m) Calculated value σ	Rim Elevation (m) Calculated value σ	Crater Elevation (m) Calculated value σ	H_{Co} (m)	W_{Co} (m)	W_{Cr} (m)	D_{Cr} (m)	W_{Cr}/W_{Co}	H_{Co}/W_{Cr}	H_{Co}/W_{Co}
Caldera Blanca (Kervyn et al., 2012)	tuff cone				109	1555	1106	191	0.71	0.10	0.07
C27 (Brož and Hauber, 2013)	–				185	7273	3522	137	0.484	0.053	0.025
Caldereta (This work)	tuff ring	239 22	276 31	200 3	37	582	407	76	0.70	0.091	0.064
C27 (This work)	tuff ring	−2789 50	−2672 81	−2792 7	116	6362	3548.3	119	0.558	0.033	0.018

accretionary lapilli and post depositional structures, such as bomb impacts, to the top. The characteristic white and yellow tones are given by the hydrothermal alteration of the basaltic tuffs and the development of soils (Perez-Torrado et al., 2013; Lanzarote Geoparque).

The object of this study is the Caldereta volcanic edifice, located approximately 200 m to the east of Caldera Blanca, for which a hydromagmatic origin has been attributed due to its similar characteristics and because its smaller size makes a highly dense grid survey affordable (Barrera Morate and García, 2011).

3. Methodology

3.1. Morphometric analysis of the volcanic edifices

We have used different data sets to conduct the morphometric analysis. In the case of Mars, the data come from the Context Camera (CTX) instrument (Malin et al., 2007), whose images, with a spatial resolution of 5 m/px, have been used to also carry out the Digital Terrain Models (DTMs) that have been processed with the MarsSI (marssi.univ-lyon1.fr) application and have a mesh pitch of 12 m. To carry out the measurements corresponding to the Earth we have used the DTM with a mesh size of 2 m (Instituto Geográfico Nacional, 2015) and the PNOA images with a spatial resolution of 25 cm/px (Instituto Geográfico Nacional, 2023), both products developed and distributed by the Instituto Geográfico Nacional (IGN).

Instead of the classical approach by Settle (1979), which stablishes the cone basal diameter as the average of the maximum and minimum base diameters, and the cone height calculated as the difference between the average basal elevation and the maximum elevation observed at the cone's rim crest, for this study we have used the following morphometric parameters to classify Caldereta and C27 (Nephentes-Amenthes Cones (NAC), Mars) volcanic edifices following Vespermann and Scmincke (2000), and to allow their comparison to other edifices from Earth and Mars (Table 1): Cone Height (H_{Co}), calculated as the difference between the average altitude of the cone and the average altitude of its base (Favalli et al., 2009). We followed this procedure because this method yields more accurate results for cones in areas with 5 % slopes, or greater, and partially buried by lava flows, as is the case of Caldereta volcano (Fig. 2). Cone basal width (W_{Co}) and crater width (W_{Cr}), have been estimated as the diameter of an equivalent area circle outlining the base of the volcano or the crater rim respectively. In both cases, the circle has been extrapolated for completion as the volcanoes show a horseshoe shape. Crater depth (D_{Cr}) has been obtained by subtracting the minimum altitude of the crater floor from the average altitude of the cone.

This analysis has been performed on cuttings of the original raster layers with the following extensions: In the case of Caldereta volcano a cutting of the base of the edifice and a cutting of the crater rim both with a 5 m buffer for being the native pixel size of the raster of 2 m. In the case of C27 a cutting of the base of the edifice and a cutting of the crater rim both with a 20 m buffer for being the native pixel size of the raster of 12 m. This operation has been performed with the latest version of QGIS software (QGIS 3.34.3 Prizren of 19.01.2024). The cuttings have been outlined following the break of the slope between the base of the edifice and the surrounding topography, the base of the crater and the crater walls and the maximum heights of the rim. The buffers have been implemented to allow for an average calculation of heights.

3.2. Magnetometry

The system used for on board drones magnetometry is that described in Fernandez Romero et al. (2021). The platform is a Matrice 600 Pro hexacopter modified to accommodate a pod with a deployable boom as well as the auxiliary payloads to guarantee the flight conditions and perform the telemetry.

The magnetometer used is a fluxgate sensor that acquires the vector field. The instrument has <6 pT/$\sqrt{\text{Hz}}$ noise per axis. The magnetometer and the drone are rigidly attached in order to be able to derive the vector components from the attitude data of the vehicle, and the instrument is mounted in the extreme of a 1.2 m boom to minimize the magnetic field sourced by the platform. The attitude of the magnetometer is maintained in a very low angle respect to the vertical by means of a low flight speed of 1.5–2 m/s.

The flight plans consist of mapping patterns in grids with 4 straight sections of 200 m, spanning more than 1000 m of flight taking off and landing from the same point (Fig. 3). Typically, the flight operation base is located at the highest point of the rim to guarantee visual control and a correct reception of the telemetry. The length of each track was adjusted to drain it to 30 % approximately of the Lithium Polymer (LIPO) batteries for security reasons. The flights drape the terrain under measurement by means of UgCS Drone flight planning software (Sphengineering.com, 2025) in closed loop with a Attollo Engineering (WASP™-200 LRF, 2025) CU1–001 laser altimeter reading, with an estimated height error in the order of ±1 m under the present survey conditions (smooth wind conditions).

The flights are performed at 20 m height, with a 10 m spacing

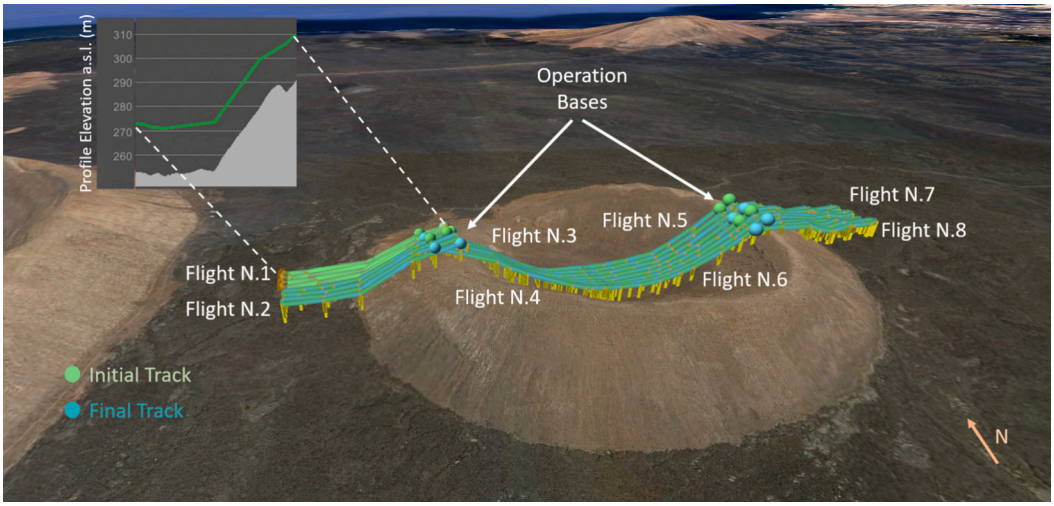


Fig. 3. Image of the Caldereta volcano with the set of NE-SO flights from UgCS software. The inset represents the profile elevation of the first flight track.

between the lines for a reasonable balance between resolution and security due to the steep slopes of the volcano rim (up to 47°, Fig. 3). The tracks have been designed with a radial pattern to register the magnetic field perpendicular to the main boundaries.

The electronic system acquires and transmits the magnetic field components to the ground station, the GPS, the compass and the IMU signals. The error of the modulus is estimated as <2 nT taking into account the standard deviation of the three components and the magnitude of the global magnetic field. The scalar information is calculated as the modulus of the field from the raw components in the drone reference system (DRS). The calculation of the anomaly has been performed taking into account the global and crustal contributions by means of the International Geomagnetic Reference Field (IGRF) model (Thébault et al., 2015) and the World Digital Magnetic Anomaly Map (WDMAM) 2.1, an evolved version of the 2.0 (Lesur et al., 2016), respectively.

Therefore, the anomaly is calculated as: $\Delta|B| = |B_{measured}|-|B_{IGRF}|-|B_{WDMA}|$, where B_{IGRF} and B_{WDMA} correspond to the two above-mentioned contributions.

The vector data in the geomagnetic reference system (GRS) are obtained after the rotation of the data in the DRS according to the compass and IMU information. The error estimated is 200 nT and 160 nT for the horizontal and vertical components respectively. Vector data have been corrected with the IGRF model to calculate the anomaly. A further correction of the vector data with the crustal model is not possible since this model provides only modulus information.

The graphical representation of the data in the present work results from a moving average filter of 1 % selected for smoothing the signal from short wavelength fluctuations.

3.3. Modeling and validation method

In the absence of electrical currents, the magnetic field sourced by a set of magnetized rocks can be considered a potential field (Reitz et al., 2008). The model created for the inversion is thus, based on the magnetic charges or poles of the different elements, and the calculation of the field is conducted through the scalar magnetic potential (Díaz Michelena et al., 2022).

The geometry of the structure to model is built by means of simple geometrical bodies which try to reproduce the observed morphology. During the modelisation a remanent magnetization (Mx, My, Mz) in A/m is attributed to the bodies based on the reference values of samples collected in the terrain and measured with a Vibrating Sample Magnetometer (VSM), which range between 1.49 and 9.82 A/m. The problem consists in seeking the magnetization that minimizes the error function between the measured and calculated magnetic fields.

The digital elevation model of Caldereta volcano resembles a circular corona body with an altitude in the order of 300 m and with 400 and 600 m internal and external diameters that lacks a sector in the order of 45° in the North-western side. To reproduce this shape, and with the assumption that every dipole resides on the surface, two bodies have been used: 1) a circular corona of 70 m height of 300 and 600 m internal and external diameters, respectively; and 2) a corona sector of 45° with the same internal and external diameter dimensions (Fig. 4).

The corona will be attributed the average magnetic susceptibility of the Caldereta rocks and is magnetized in the direction of the geomagnetic field, while the sector will be magnetized in opposite direction.

The susceptibility (χ) attributed to the bodies is 0.142 S.I., and the magnetization is calculated as (Mx, My, Mz) = χ (H, 0, Z) being H and Z the horizontal and vertical components of the geomagnetic field according to the IGRF model: H = 24.7 A/m, and Z = −19.0 A/m (pointing towards the geographic North and outside of the Earth center respectively). Therefore: (Mx, My, Mz) = (3.5, 0, −2.7) A/m, and the resulting magnetization is 4.42 A/m, which is in good agreement with the obtained NRM values.

For simplicity, the calculation has been performed at an altitude of 20 m from the highest elevation point of the volcano. The modeling is conceived to resemble the terrain draping of the survey flights in the rims with a constant distance between it, the source, and the calculation

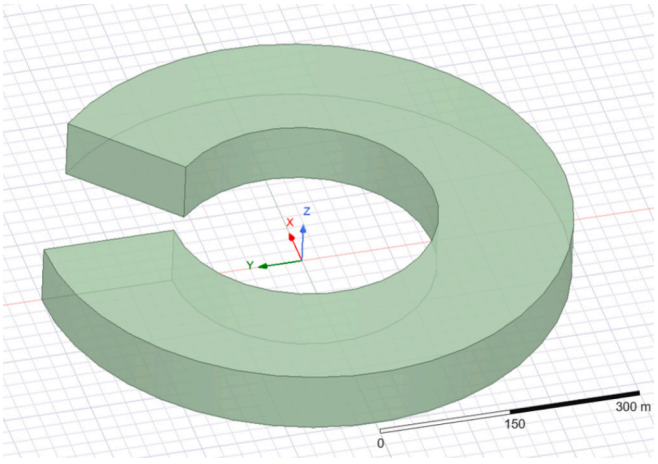


Fig. 4. Simulated Caldereta volcano structure. The cylindrical corona is 70 m high and has internal and external radii of 150 and 300 m respectively. A magnetization of 4.42 A/m in the present direction of the geomagnetic field in the area is assigned.

height of 20 m, while the distance of the numerical simulation to the ground in the central and outer parts of the crater is 90 m.

This represents a limitation for the intercomparison of the data, which have been obtained at a constant altitude of 20 m from ground. Despite of this fact, the computation is considered to be qualitatively representative since the distance is lower than the crater dimension.

A quantification of the results can be performed between the zones in which the calculation has been done in the same conditions as for instance an intercomparison of the inner part of the crater. In order to quantify the reliability of the models the experimental measurements have been interpolated to obtain the values of a regular grid, allowing to a direct comparison between experimental and synthetic data.

4. Results

4.1. Geomorphology

For the study and appropriate description of Caldereta volcano and its comparison with potential hydromagmatic volcanos in Mars we have performed the geomorphological analysis described in the methodology section, whose results are depicted in Table 1.

Caldereta volcano is a horseshoe shape monogenetic edifice with the small opening facing the NW (Fig. 5). It presents an average height of 37 m, an average crater diameter of 407 m and an average height/rim diameter (H_{Co}/W_{Cr}) aspect ratio of 0.091 (Table 1).

These features are compatible with those of tuff rings following Vespermann and Scmincke (2000), aka. Heights less than 50 m, crater diameter between 0.2 and 3 km and a height/rim diameter between 0.13 and 0.05. The high W_{Cr}/W_{Co} (=0.69), very similar to that of Caldera Blanca (Table 1), could support that the two structures had a similar

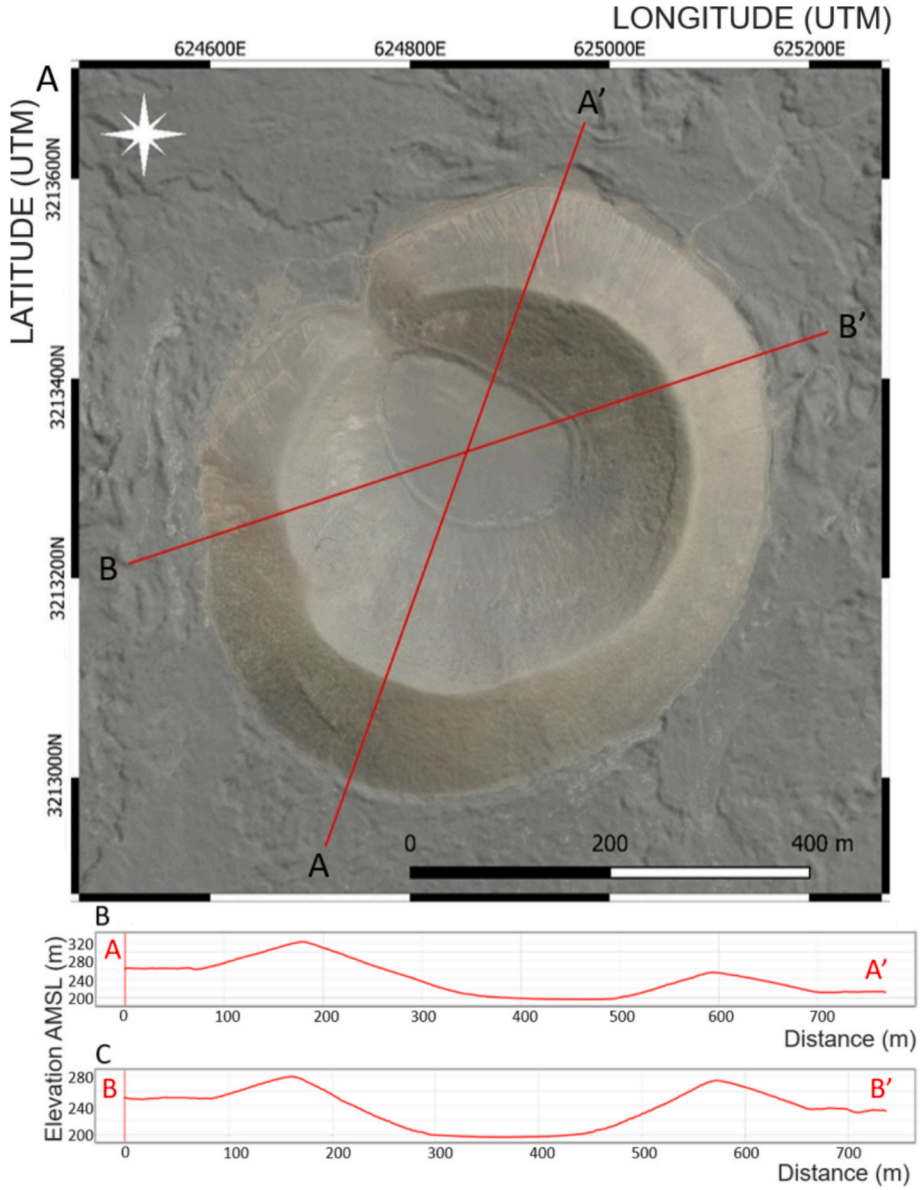


Fig. 5. A. ESRI satellite image of Caldereta volcano over a Digital Elevation Model (resolution: 2 m). Red lines are A-A' and B-B′ are the two elevation profiles depicted under the image (B and C respectively). The direction of the profiles corresponds to the flight direction of the hexacopter drone in the measurement campaigns (N21.2°E for A-A' and N72.8°E for B-B′). (For interpretation of the references to colour in this figure legend, the reader is referred to the web version of this article.)

eruption process.

The martian feature chosen for comparison with Caldereta is crater C27 (107.32°E/16.57°N) from Nephentes-Amenthes region. This crater is, like Caldereta, a horseshoe shape edifice with the opening facing east (Fig. 6). Its average height is 116 m and displays an average crater diameter of 3548 m, values that correspond to an average height/rim diameter (H_{Co}/W_{Cr}) aspect ratio of 0.033 (Table 1).

4.2. Magnetometry

The results are obtained after a 5-day survey that comprised 42 flights, which covered a distance of 40 km (drone magnetometry) and an extension in the order of 50 ha.

Fig. 7 shows a map of the magnetic field of Caldereta tuff ring, recorded by the drones. The magnetic anomaly shows two dipolar anomalies, each located at opposite rims.

4.3. Numerical models

4.3.1. Caldereta volcano

Fig. 8. shows the superposition of the simulated magnetic field and the observed data using the drone magnetometery system.

The individual patterns of the magnetic anomaly resulting from the interpolation of the experimental values as well as the synthetic data are shown in Fig. 9. As expected, the matching is best in those areas where measurements are available and therefore, where the interpolation casts the signals of the edifice.

An analysis of the quadratic residual absolute value between the measurements and the simulated values (Fig. 10 A and B respectively) results in a negatively-shifted normal shaped distribution centered in −45 nT.

The horizontal and vertical components of the magnetic field have also been obtained for the experimental values and computed numerically. Results are represented in Figs. 11 and 12 for the horizontal and vertical components of the magnetic field respectively.

Fig. 11 shows the experimental values of the vector components for Caldereta volcano. In both cases the contrast drapes the physical interfaces of the volcano. Fig. 12 depicts the synthetic values. The dotted line is the contour of the modeled structure in order to appreciate clearly how the contrast is associated to the physical interfaces.

As it is the case with the scalar data, the horizontal and vertical components of the model are in good correlation with the experimental values.

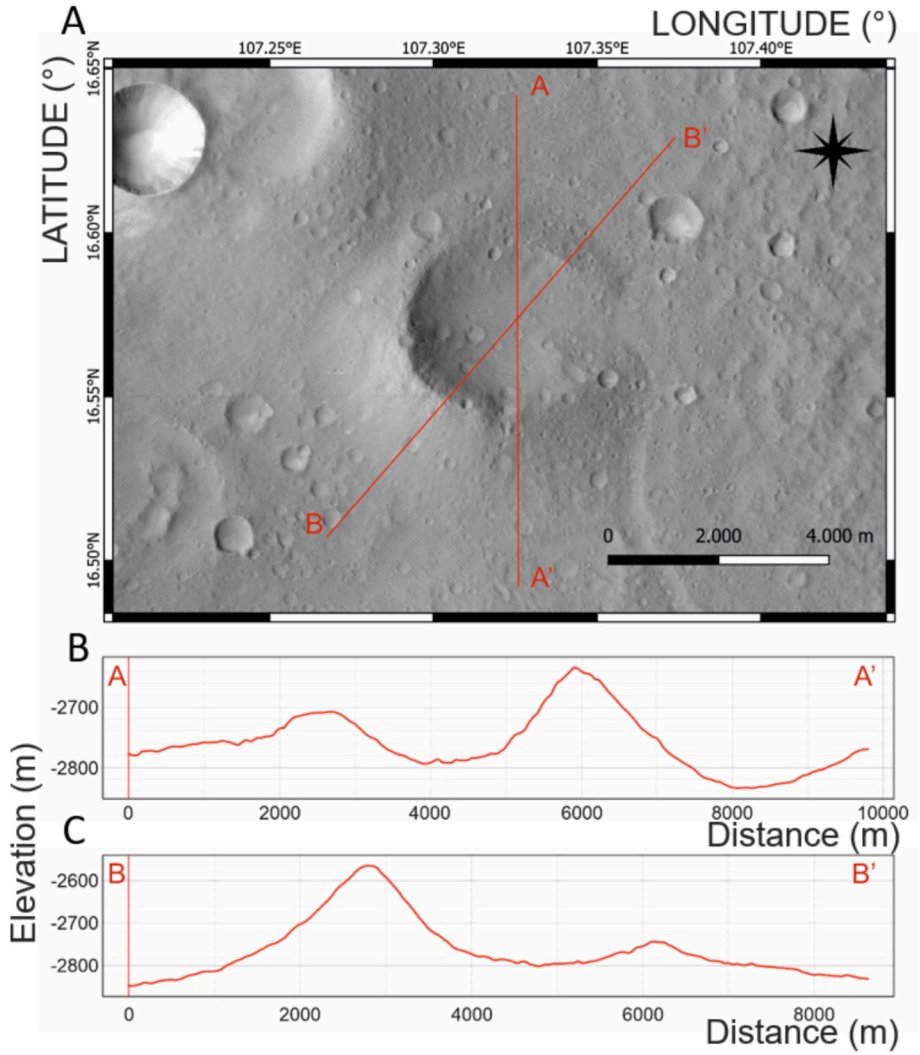


Fig. 6. A. Context Camera (CTX) image of C27 crater (spatial resolution of 5 m/px) over a DTM processed with the MarsSI application. Red lines A-A' and B-B′ are the two elevation profiles, referred to datum Mars 2000, depicted under the image (B and C respectively). The parameters of C27 with our measurements are similar to the ones given by Brož and Hauber (2013), which validates our measuring procedure. (For interpretation of the references to colour in this figure legend, the reader is referred to the web version of this article.)

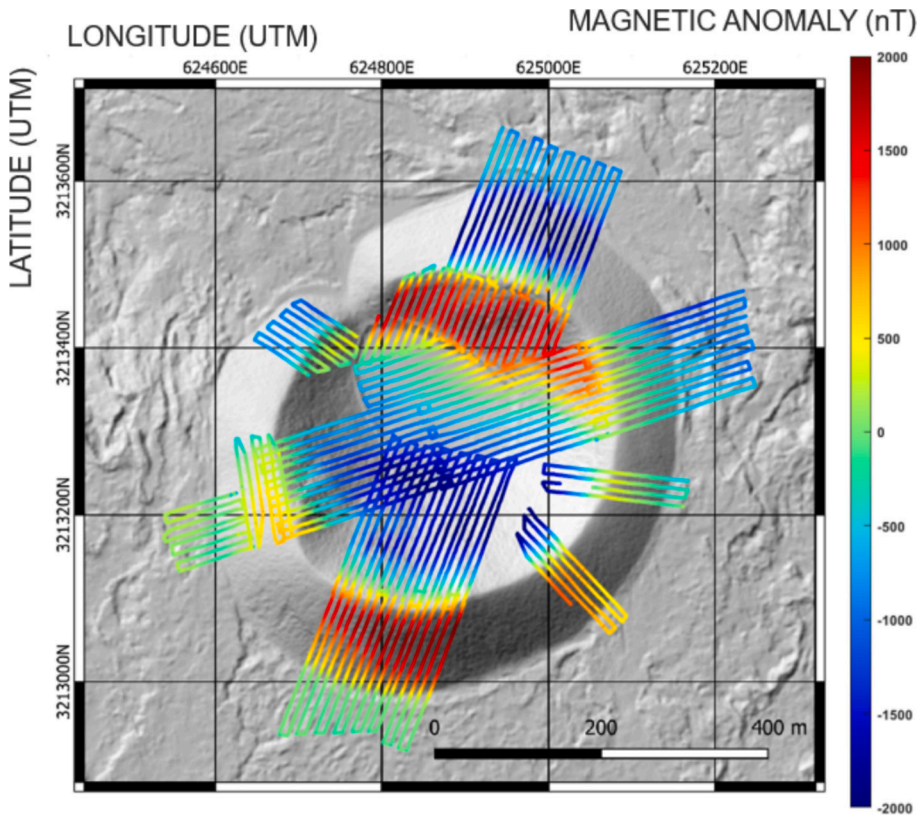


Fig. 7. Magnetic field anomaly of Caldereta volcano obtained with the drone measurements superimposed with the above-mentioned Digital Elevation Model (DEM).

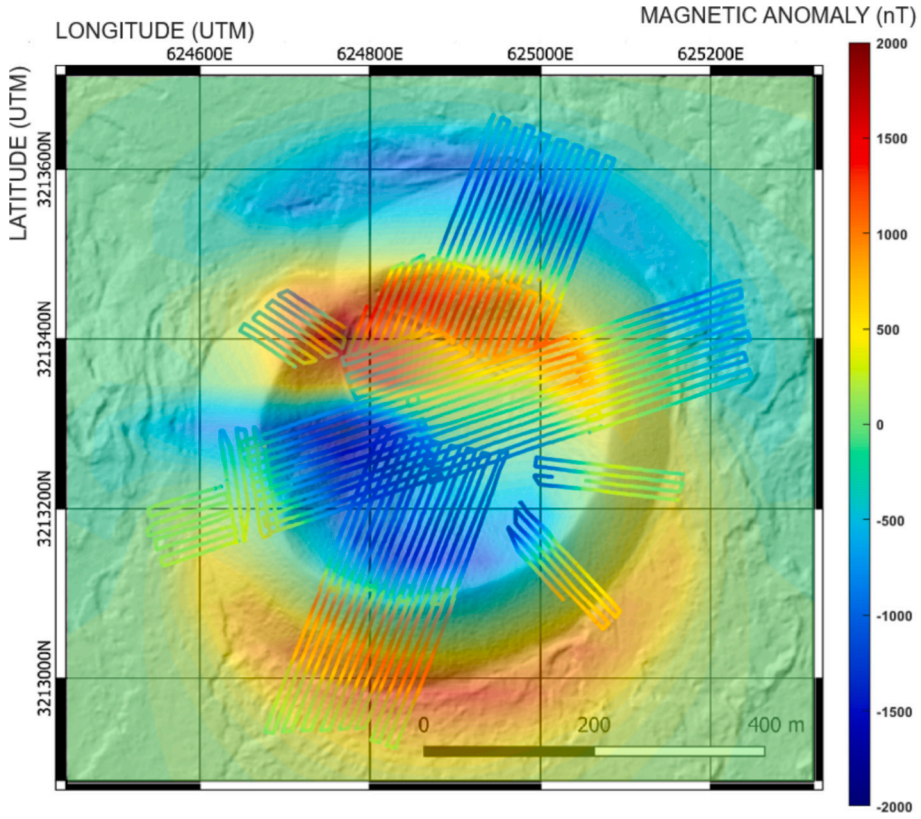


Fig. 8. Superposition of the Caldereta magnetic field anomaly experimental and synthetic data of Caldereta volcano and the superimposed with the above-mentioned Digital Elevation Model (DEM).

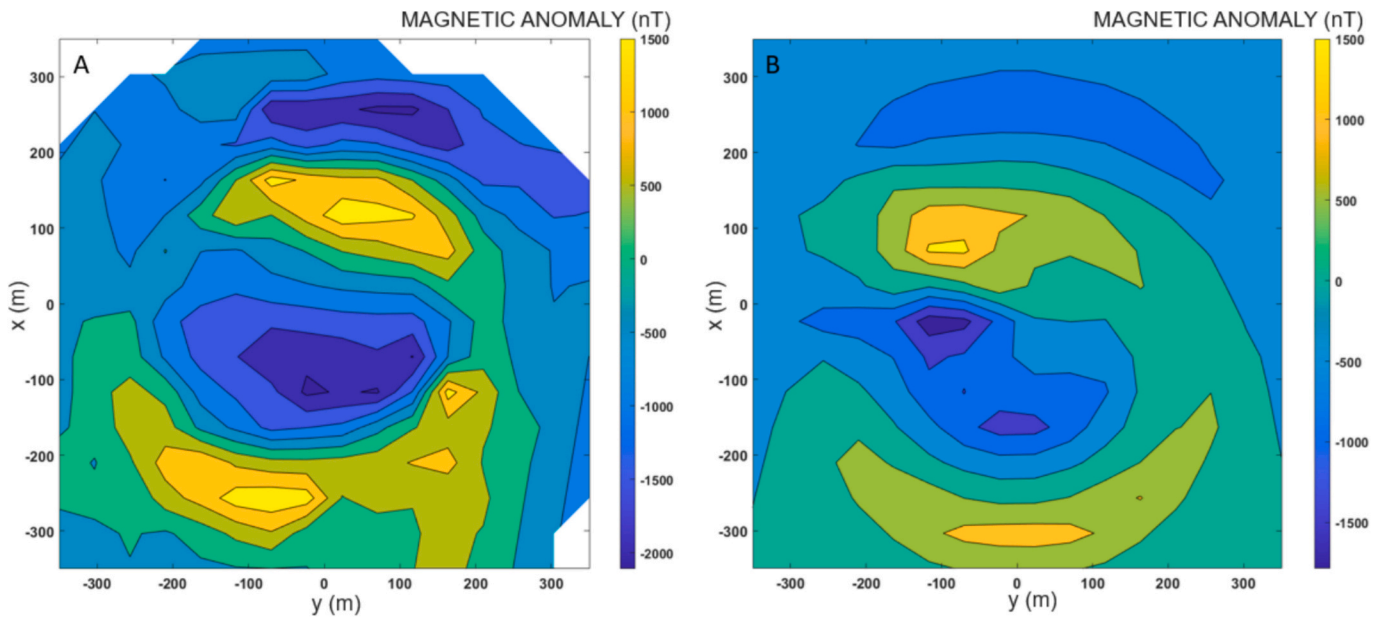


Fig. 9. A.Interpolation of experimental measurements, and B. Interpolation of simulation values.

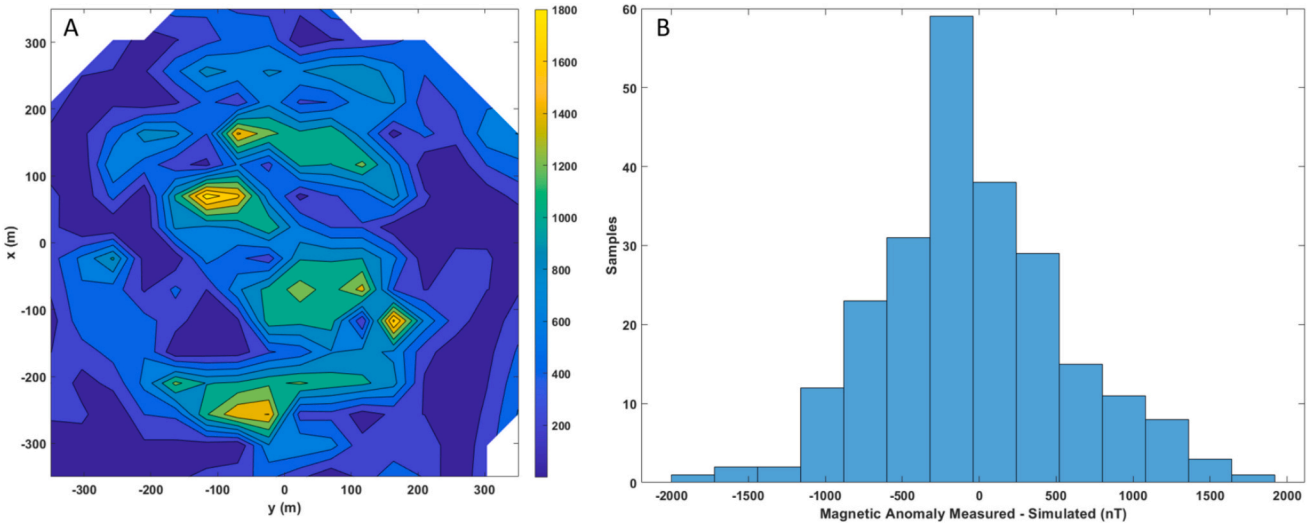


Fig. 10. A. Data distribution of the quadratic residual absolute value and B. graphical representation of the difference between experimental and simulated values.

4.3.2. C27 volcano

A similar model has been computed for the C27 volcano based on the Caldereta one. The crater has been modeled analogously as an open ring corona of 1774 and 3181 m internal and external radii respectively and with an aperture towards the East of 25°. For this model, the topology of the magnetic field of Mars has been assimilated to that of the geomagnetic field. Therefore, for the latitude of the C27, the inclination of the field is in the order of −45°. Two models have been computed: one, under the assumption that the eruption took place when the magnetic field was still active, and another one assuming a later formation. For this last case, the surroundings of the crater have been uniformly magnetized to highlight the contrast of an eruption whose products do not magnetize when they cool down.

In the first model, the body has been attributed a magnetization of 3.16 A/m for the horizontal component and − 3.1 A/m for the vertical one. The anomaly has been calculated at a height of 200 m due to the large dimensions of the crater in comparison with Caldereta one, in present time when the magnetic field is extinct. The result is shown in Fig. 13.

For the second model the body is not attributed any magnetization. The results are shown in Fig. 14.

5. Discussion

In this section we discuss the question of the appropriateness of Caldereta volcano as a terrestrial reference and its comparison with C27 martian crater; on the suitability of the magnetometry with drones as a geophysical tool to identify hydromagmatic eruptions and the capability of the mathematical models to derive such information in planetary studies.

5.1. Case studies in Earth and Mars: Caldereta and C27

On Earth, Caldereta has been classified as hydromagmatic (García Cacho and Romero, 2000), and grouped along with the eight volcanic centres of Caldera Blanca/ Risco Quebrado volcanic system in

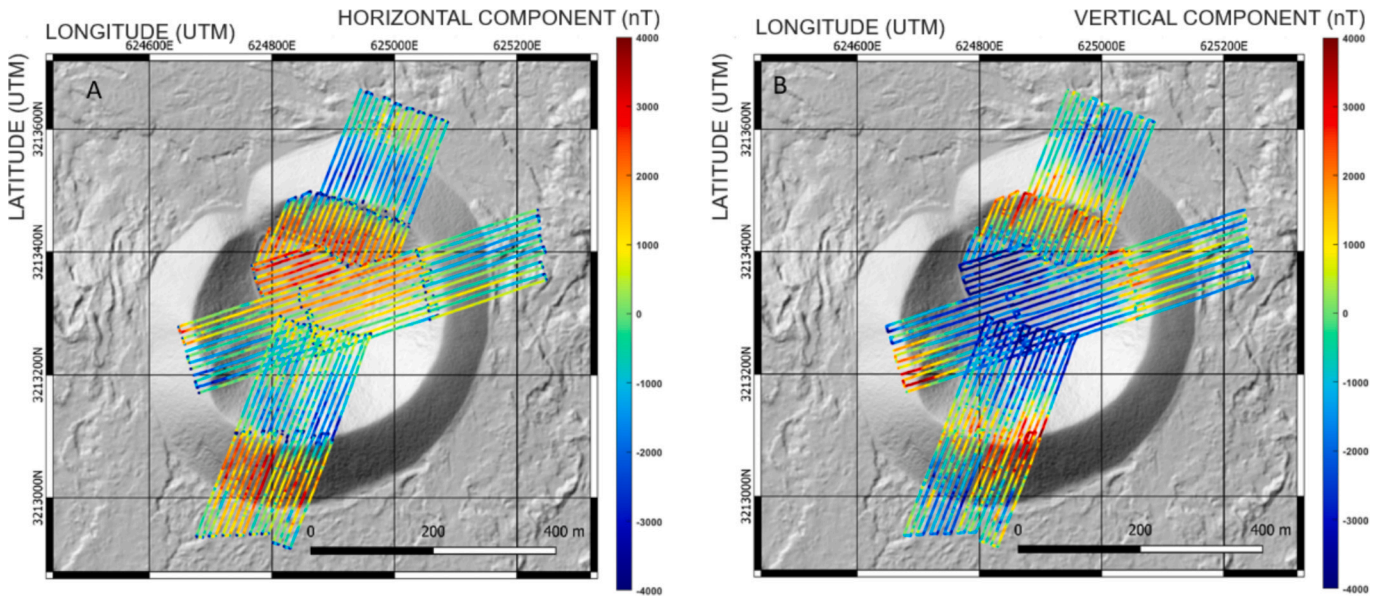


Fig. 11. Horizontal (H) and vertical (Z) components of the anomaly measured with the drone system.

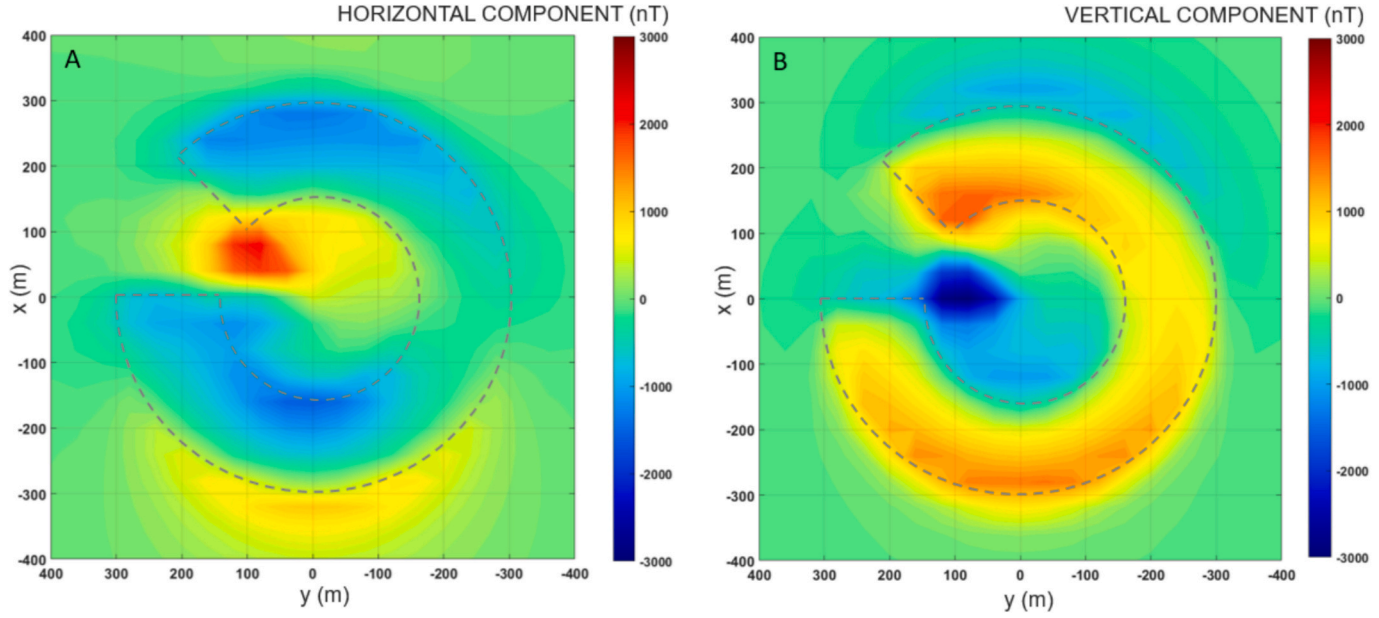


Fig. 12. Mathematical simulation of the magnetic field anomaly horizontal (H) and vertical (Z) components. Dotted line represents the contour of the circular corona used to mimic the morphology for the model.

Lanzarote, the Easternmost island of the Canary archipelago in Spain, for their similar volcanological characteristics and their stratigraphical position in relation with other nearby eruptions (Barrera Morate and García, 2011).

On Mars, based on a detailed morphological and morphometrical study of the edifices and an analysis of the regional context, Brož and Hauber (2013) attributed a hydrovolcanic origin to the pitted cones in the Nephentes/Amenthes region, which were previously interpreted as mud volcanoes (Skinner Jr and Tanaka, 2007).

Among the edifices studied by them, we have selected C27 edifice for its morphological similarity to Caldereta. Both have a horseshoe shape and display high crater to cone base ratios with well-developed deep and wide craters. As mentioned before, Caldereta volcano falls in the tuff ring category from Vespermann and Scmincke (2000) but, as the elevation of its crater base (200 m) seems to be below the average elevation of the base of the edifice (239 m), we could argue that it belongs to the maar category, given that tuff rings and maars have a similar morphology with the difference that in maars the crater is cut into the pre-eruption surface (Vespermann and Scmincke, 2000). This asseveration cannot be unequivocally proven though, given the lack of information about the uneven thickness of the Timanfaya lava flows around Caldereta that hamper a precise knowledge on the original topography around the volcano at the time of its formation.

The main difference between these two edifices would be the larger size of C27. Martian volcanoes tend to be taller, have a larger basal diameter (W_{Co}) and gentler slopes (<30°) than Earth ones due to the lower values of gravitational acceleration and atmospheric density in Mars (Brož et al., 2015). For this reason, we plot in the broadly used W_{Cr}/W_{Co} ratio versus W_{Co} diagram (e.g. Pike, 1978; Hasenaka and Carmichael, 1985) (Fig. 15) to compare this two edifices to other

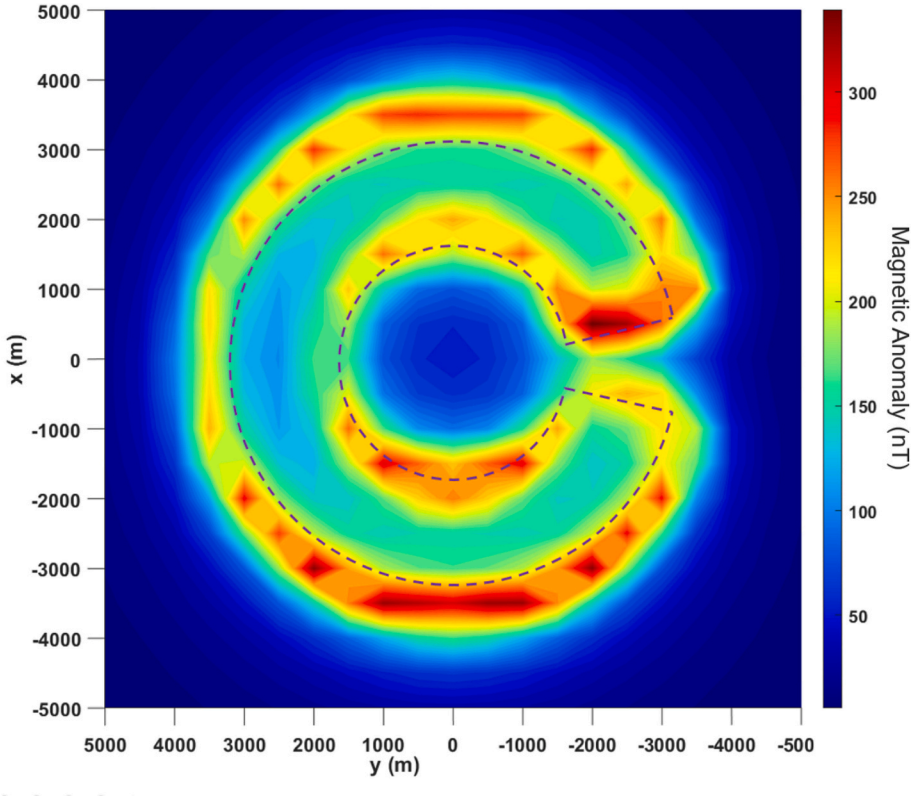


Fig. 13. Mathematical simulation of the magnetic field anomaly of C27 crater under the assumption that the global magnetic field of Mars had a similar intensity and topology of that of the Earth and therefore, H = 34,414 nT, Z = -35,112 nT. Dotted line represents the contour of the circular corona used to mimic the morphology for the model.

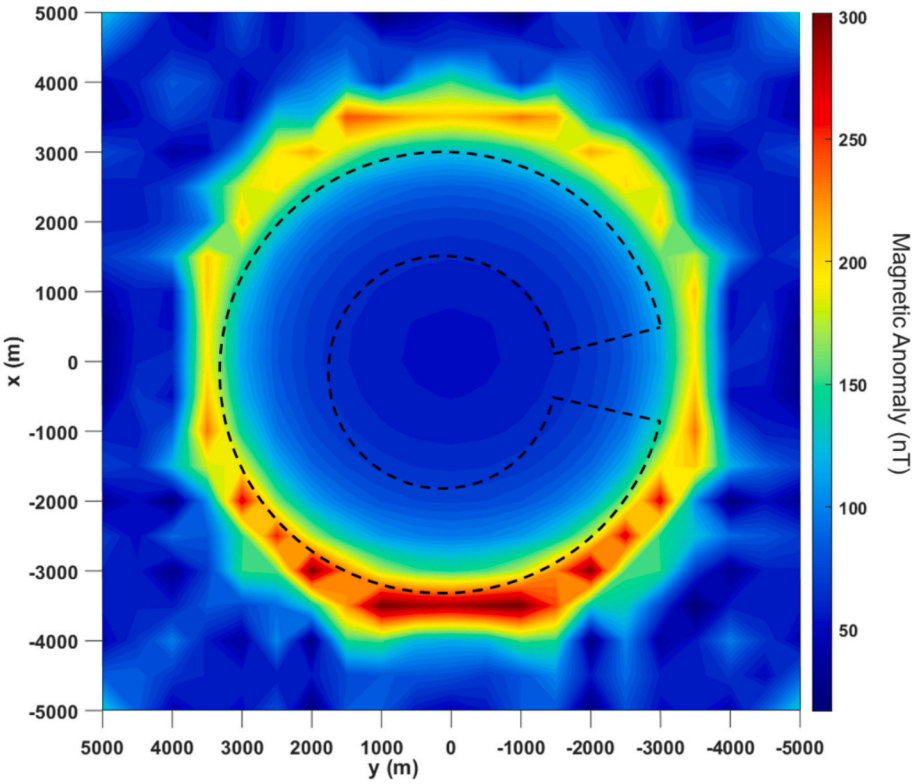


Fig. 14. Mathematical simulation of the magnetic field anomaly of C27 crater under the assumption that the global magnetic field of Mars had been vanished by the time of the eruption. Dotted line represents the contour of the circular corona used to mimic the morphology for the model.

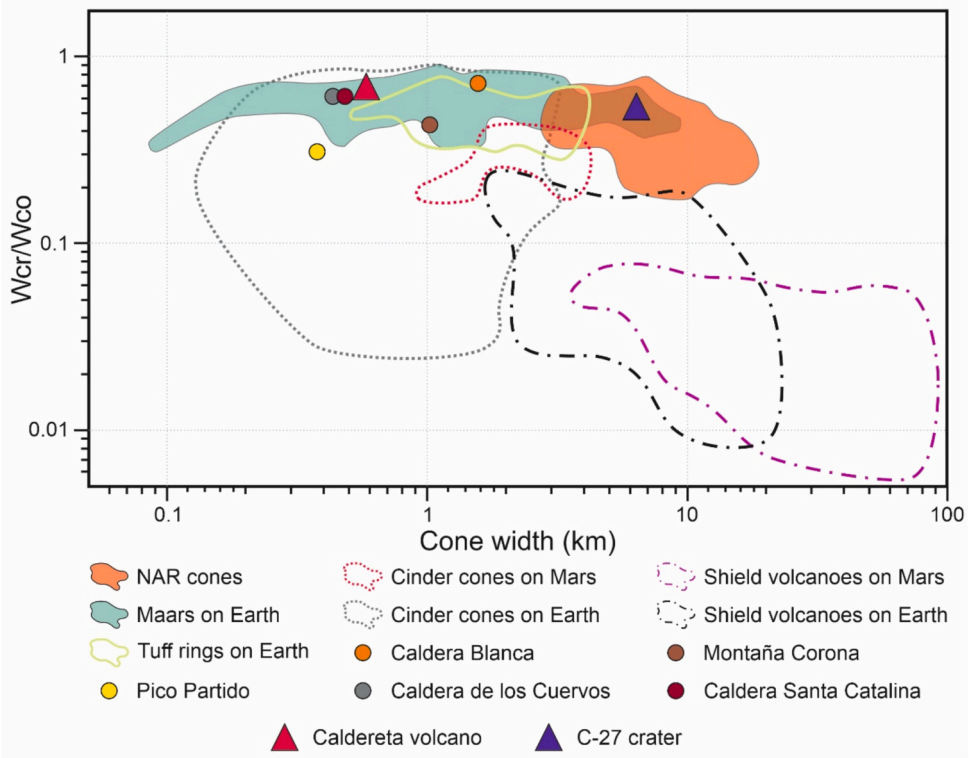


Fig. 15. Comparison of Caldereta volcano to other types of terrestrial and martian volcanic features on a Wcr/Wco vs. basal width (Wco); modified from Brož and Hauber (2013). NAR cones (orange area) data from Brož and Hauber (2013); Maars on Earth (green area) data from Pike (1978); Tuff rings on Earth (continuous yellow line) data from Pike (1978); martian cinder cones (Ulysses Colles) (dashed red line) data from Brož and Hauber (2013); Cinder/scoria cones on Earth (dashed grey line) data from Hasenaka and Carmichael (1985), Pike (1978) and Inbar and Risso (2001); Shield volcanoes from Mars (dashed purple line) data from Hauber et al. (2009); Circles: Lanzarote volcanic edifices, data from Kervyn et al. (2012); Red triangle: Caldereta volcano (this study); Purple triangle: C27 crater on NAC field (Mars) (this study). (For interpretation of the references to colour in this figure legend, the reader is referred to the web version of this article.)

martian and terrestrial volcanoes and to confirm the validity of our measurements by comparing C27 parameters to those performed by Brož and Hauber (2013) on the same edifice.

As shown in Fig. 15 different volcanic types on Earth and Mars are displayed at distinct areas, with the expected displacement of martian volcanoes towards higher values of cone width in comparison to terrestrial volcanos of the same type due to their bigger sizes. The location of C27 with our measurements is similar to the Brož and Hauber (2013) ones, which validates our measuring procedure. As previously suggested, Caldereta plots within the field of Earth maars, together with other volcanos from Lanzarote. C27 on the other hand, plots among the other cones from NAR, described by Brož and Hauber (2013) as hydromagmatic. Therefore this two edifices seem to be hydromagmatic, specifically maars, and therefore are well suited for our comparison study of their magnetic signature.

5.2. *Methodology of magnetometry and modeling*

This methodology comprises experimental in situ surveys and morphometric analyses as well as the development of mathematical models based on simple geometrical volumes that mimic the morphology.

The main experimental sources of error are the uncertainties and noise of the magnetometer, the disturbance by the platform, the positioning and attitude errors of the GPS and the IMU, and the flight altitude determination by the laser altimeter. The principal sources of error of the mathematical simulations are the geometrical differences between the volcanoes and the models, the hypothesis on the body magnetization, and the relative altitude of the flights. The positioning is considered appropriate for structures of the order of hundreds of m since the GPS error is 1.5 m. The errors of the measured magnetic field associated with the instruments have been computed as tens of nT for the modulus and hundreds for the vector components. This is considered suitable for the analysis of this structure with a notable signature with amplitude of ±1500 nT.

The effect of the magnetic fields induced in the drone have been mitigated with the deployment of the magnetometer in a 1.2 m boom. This measure is effective in the determination of the modulus. However, the effect of the flight attitude can be appreciated in the turning points of the H and Z components, where some spurious anomalies appear. Regarding the vector information, it can be highlighted that it is very affected by the relative orientation of the drone with respect to the present geomagnetic field. This effect has to do with the fact that the Earth magnetic field may induce a magnetization in some parts of the drone and as a result, this parts would produce a varying interfering magnetic field in the position of the magnetometer. For features which raise lower magnetic contrast, the vector data would only be useful with an improved attitude determination, and especially a better IMU.

In relation to how the mathematical model emulates the structure under study there are several factors. Based on the morphometric analyses, a simplified volume of open ring coronae has been used to mimic their bodies for the numerical models that compute the magnetic field. Caldereta volcanic structure has 300 and 150 m external and internal radii. The corona lacks a 45° wedge to mimic the horseshoe shape. The model has been attributed a magnetization of 4.42 A/m compatible with measurements of collected samples performed at the laboratory.

The field sourced by the structure is proportional to its magnetic moment and this is proportional to the magnetization and the volume. The volume calculated with the DEM varies between 11.1 and $13.5 \cdot 10^6$ m^3, depending on whether the ground level is taken at the lowest point within the crater or at a 10 m height respect to this point. The volume of the simulated structure is $13 \cdot 10^6$ m^3. This volume would fit in that range

(errors comprised between −1.9 and $0.5 \cdot 10^6$ m^3) which would consider, at least partially, a higher ground level of the surroundings, which cannot be determined due to the uncertainty of the Timanfaya lava thickness. To show this difference, we have graphically compared the profiles of the volcano and the model along the A-A' and B-B′ transects (Fig. 16). In the A-A'transect the model profile area exceeds that of the edifice in a 7 %. In the B-B'transect the model profile has a defect of area respect to the edifice of 5 %, which compensates between each other.

Another aspect is the flight draping of the terrain and the altitude of the magnetic field computed, which is constant. Several simulations run at different altitudes provide similar results in a range of tens of m, which only affect the intensity and not the aspect of the anomaly. Differences start to be important when the altitude of the simulation differs in hundreds of m respect to the flight. There is a deviation of the vector components due to the different angle of the magnetometer with the exposed surface in both scenarios. As the attitude of the flight is constant, the boom, to which the magnetometer is attached, remains in a vertical position and yields different angles with respect to the terrain. However, in the simulation the angle between the payload and the surface is straight and constant (Fig. 17).

This affects in a greater extent the vector components: the poles reflected by the Z component in the model have a higher extension than the experimental values. In the H component the transition of the experimental values is also more progressive along the slope of the rim.

Despite of these differences, the magnetic field intensity computed by the simplified model fits very well with the experimental values in intensity and shape of the dipoles with very low residual values.

Additionally, the residuals between the experimental values and the simulation (Fig. 10) have been carefully analyzed to find extra dipoles, which could delineate secondary structures which could have slowly solidified and acquired a magnetic order in the center of the crater. Due to the absence of such dipoles, an order in depth has been discarded, which is compatible with a maar diatreme structure that is filled with fragments of rocks associated to the phreatomagmatic eruption and doesn't preserve the feeder dyke.

This result proves that the methodology of survey and modeling is adequate for such kind of structure preliminary classification. Furthermore, due to the simplicity of the model it can be very well adapted to different studies with low computational times and therefore even used for real time verifications during the field campaigns and to refine the field planning.

5.3. Analysis of the magnetic signatures

The scalar and vector information casted by the results in Caldereta indicate that the magnetization has the direction of a direct geomagnetic field. This is compatible with the estimated age of the structure (< 2 Ma). Furthermore, because the geomagnetic field in the period between 2 Ma ago and 690,000 ka has been dominated by reversed geomagnetic field, the fact that the magnetization is direct helps to constrain the eruption in the periods between 1.98 and 1.95, 1.79 and 1.64, 1.63 and 1.61 and 0.95 and 0.89 Ma ago (Cox, 1969).

At present there is no available dating for C27. In the case that these craters are indeed volcanic and were formed in a period when the global magnetic field of Mars was still active, the crater would have acquired a magnetization whose intensity would depend on factors such as the magnetic carriers' percentage and remanence, as well as the cooling speed. In the case that the eruption had taken place after the magnetic field vanished, the products of the eruption would not magnetize and therefore, the signature would be that of a demagnetized spot.

5.4. Implications on Mars ancient field

The study of the magnetic signature as a whole gives hints on the environmental field. Firstly, the expected magnetic anomaly is completely different for the two different scenarios: whether the eruption took place in the presence or in the absence of a magnetic field. Secondly, the shape of the signature gives constraints on the topology of the magnetic contrast and its intensity, together with basic information on the eruption products that can be directly associated to the magnitude of the field. To explain this aspect, in the following we focus on the modeling results intercomparison for the case in which C27 eruption occurred under the exposure of the Mars ancient magnetic field.

The main difference that can be highlighted is related to the values of the calculated field. The intensity of the anomaly is higher for the model of Caldereta because the computation height is one order of magnitude smaller: 20 m for Caldereta and 200 m for C27. This has to do with the concept of the model and the dimensions of the craters, which has a limitation with the computation distance and size and number of the elements for the grid. Additionally, it can be remarked that the anomaly in the case of Caldereta shows areas with positive and negative values. This has to do with the way the anomaly is computed as the difference between the moduli. Because of this, and due to the extinction of the martian field, the magnetic anomaly of C27 would show only positive

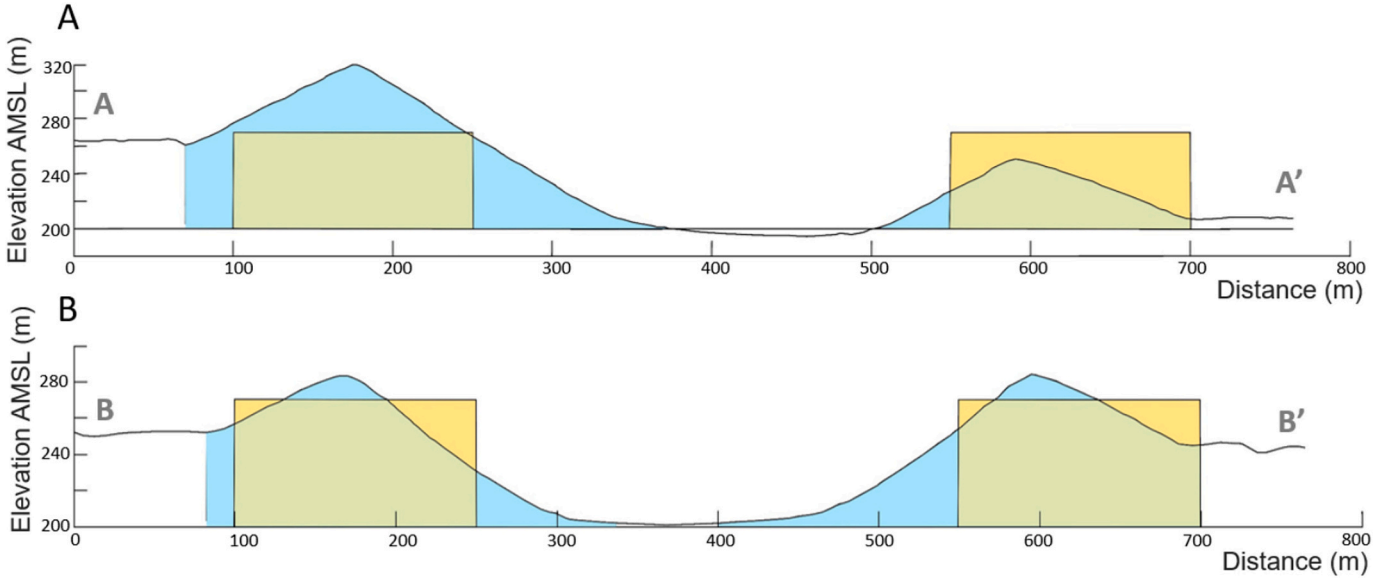


Fig. 16. Graphical representation of the profile difference between the edifice and the simulated structure along the transects A-A' (A) and B-B′ (B).

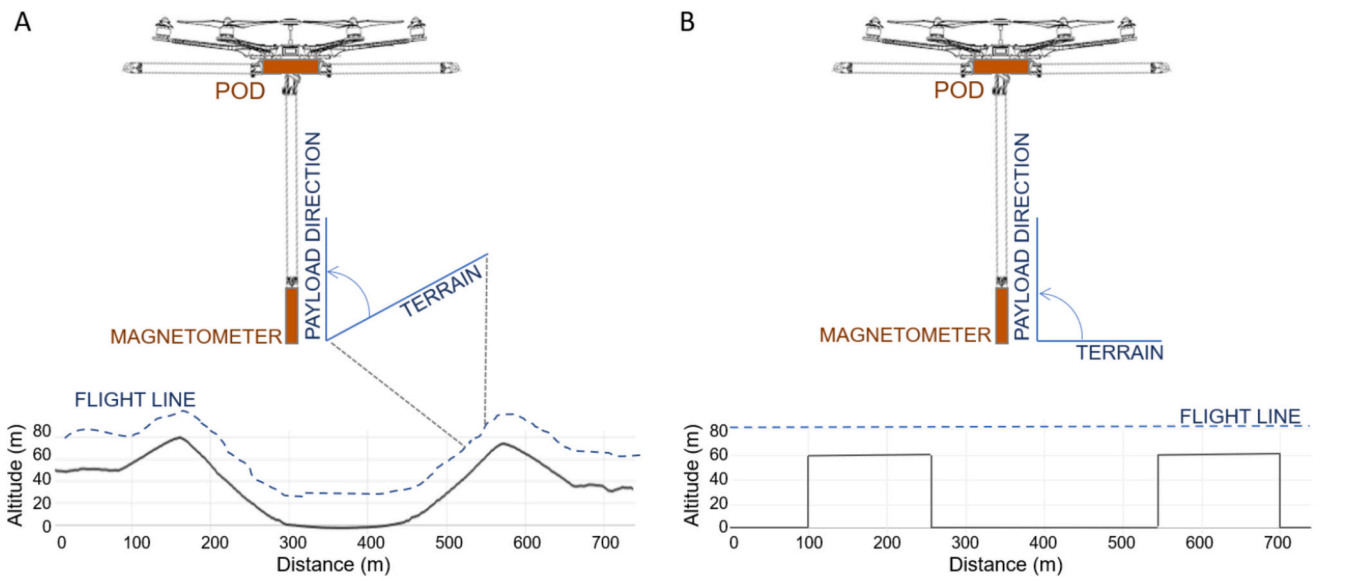


Fig. 17. Graphical representation of the flights over the terrain and the relative angle of the payload and the terrain during the flights for the experimental (A) and simulated (B) data.

values. Furthermore, the same anomaly pattern would be expected if the eruption would have taken place during a reversal of the global field.

Regarding the patterns of the anomaly there are notorious differences in their shapes. In the Earth, the core field lines are perpendicular to the surface in the poles and describe an arch between the poles. If the feature under study were located on one of the poles its stray field would present radial symmetry. However, and also related with the size of the core, at intermediate latitudes, the radial symmetry is broken into an axial symmetry due to the inclination of the field lines. This effect and its modulation along the latitude is common in the magnetic anomaly map of both Caldereta and C27 in Mars for which the magnetizing field shape is assimilated to that of the geomagnetic one.

Caldereta latitude is in the order of 30°N while C27 latitude is in the order of −16.5°N. In the case of the former, the horizontal component slightly dominates respect the vertical one and this gives rise to an elongated signature whose principal anomaly is shifted and goes beyond the morphology of the crater. In contrast, in the case of the latter, where the horizontal and vertical components are practically balanced, the signature does not extend that much outside of the crater. This kind of information is useful to constrain not only the surface characteristics of the field but also about the martian core characteristics.

6. Conclusions

This work comprises an investigation of the Caldereta hydromagmatic volcano, in the Canary Islands in Spain, as a potential analogue of other similar edifices on the Red Planet, and its comparison with C27 volcano in the NAR region of Mars catalogued as phreatomagmatic. The investigation comprises geomorphological metrics, vectorial magnetic surveys on foot and on-board drones and mathematical modeling.

The morphometric analyses permit classifying both structures as tuff rings and more specifically maar structures. As a result, Caldereta can be considered a representative terrestrial analogue of C27. The surveys provide an extensive and dense grid of the crater that allows to have a global idea of its magnetic signature. Furthermore, the experimental data cast vector information, which can be used for a fine analysis of the different components. With the aim to compute the magnetic signature of the C27 crater on Mars, a mathematical model has been constructed on a simplified structure based on the morphometric analyses of both craters. The intercomparison between them highlights the difference in the environmental conditions during the formation of both craters, which has potential application in the understanding of the ancient field of Mars and its evolution. This study can serve as a reference for the future magnetic surveys of Mars with magnetometers on board helicopters or drones.

CRediT authorship contribution statement

Marina Díaz Michelena: Writing – review & editing, Writing – original draft, Validation, Supervision, Project administration, Methodology, Investigation, Funding acquisition, Formal analysis, Conceptualization. **Emma Losantos:** Writing – review & editing, Writing – original draft, Methodology, Investigation, Formal analysis. **Miguel Ángel Rivero:** Software, Methodology, Conceptualization. **Joana Oliveira:** Writing – review & editing, Investigation, Funding acquisition. **Óscar García Monasterio:** Resources. **Federico Mansilla:** Investigation. **Ángel Melguizo:** Investigation. **José Luis García Bueno:** Resources. **David Salamanca:** Visualization. **Sergio Fernández Romero:** Writing – review & editing, Writing – original draft, Software, Project administration, Methodology, Formal analysis.

Declaration of competing interest

The authors declare the following financial interests/personal relationships which may be considered as potential competing interests:

Emma Losantos reports financial support was provided by Spain Ministry of Science and Innovation. Joana Oliveira reports financial support was provided by European Commission. Oscar Garcia Monasterio reports was provided by Spain Ministry of Science and Innovation. If there are other authors, they declare that they have no known competing financial interests or personal relationships that could have appeared to influence the work reported in this paper.

Acknowledgements

This work has been funded by the Spanish Programme for Research, Development and Innovation under the grant of references ESP2017-88930-R and PID2020-119208RB-I00: MagAres and MINOTAUR respectively. PhD. Oliveira is funded by the European Union's Horizon 2020 research and innovation programme under the Marie SklodowskaCurie grant agreement SIGMA no 893304. Data have been

processed with the MarsSI (marssi.univ-lyon1.fr) application founded by the European Union's Seventh Framework Program (FP7/2007-2013) (ERC Grant Agreement No. 280168).

The authors would like to acknowledge INTA staff for their support and, in particular, Eduardo de Diego and Pablo Morata, for their support with engineering, and María Parrondo for her support in coordination, and Thomas Francois Dominique Cornet for his support during the field campaign.

Data availability

Data will be made available on request.

References

Abdel-Monen, A., Watkins, N., Gast, P., 1971. Potassium-Argon ages, volcanic stratigraphy and geomagnetic polarity history of the Canary Islands: Lanzarote, Fuerteventura, Gran Canaria and La Gomera. Am. J. Sci. 271, 490–521.

Albee, A.L., Arvidson, R.E., Palluconi, F., Thorpe, T., 2001. Overview of the Mars global surveyor mission. J. Geophys. Res. 106 (E10), 23291–23316. https://doi.org/10.1029/2000JE001306.

Arkani-Hamed, J., 2005. Magnetic crust of Mars. J. Geophys. Res.: Planets 110 (E8). https://doi.org/10.1029/2004JE002397.

Baker, V.R., 2001. Water and the martian landscape. Nature 412, 228–236. https://doi.org/10.1038/35084172.

Barrera Morate, J.L., García, Moral R., 2011. Mapa geológico de Canarias. GRAFCAN 1, 1–6. https://www.idecanarias.es/resources/GEOLOGICO/LZ_LITO_unidades_geologicas.pdf.

Brož, P., Hauber, E., 2013. Hydrovolcanic tuff rings and cones as indicators for phreatomagmatic explosive eruptions on Mars. J. Geophys. Res.: Planets 118, 1656–1675. https://doi.org/10.1002/jgre.20120.

Brož, P., Čadek, O., Hauber, E., Rossi, A.P., 2015. Scoria cones on Mars: Detailed investigation of morphometry based on high-resolution digital elevation models. J. Geophys. Res. Planets 120, 1512–1527. https://doi.org/10.1002/2015JE004873.

Brož, P., Bernhardt, H., Conway, S.J., Parek, R., 2020. An overview of explosive volcanism on Mars. J. Volcanol. Geotherm. Res. 409, 107125. https://doi.org/10.1016/j.jvolgeores.2020.107125.

Carr, M.H., Head III, J.W., 2010. Geologic history of Mars. Earth Planet. Sci. Lett. 294 (3–4), 185–203. https://doi.org/10.1016/j.epsl.2009.06.042.

Carracedo, J.C., Day, S., 2002. Canary Islands. In: Classic Geology in Europe Series 4. Terra Publishing, Harpenden, Hertfordshire, p. 294.

Cox, A., 1969. Geomagnetic reversals. Science 163, 237–245.

Díaz Michelena, M., Kilian, R., Rivero, M.Á., Fernández Romero, S., Ríos, F., Mesa, J.L., Oyarzún, A., 2022. Magnetometric surveys for the non-invasive surface and subsurface interpretation of volcanic structures in planetary exploration, a case study of several volcanoes in the Iberian Peninsula. Remote Sens. 14, 2039. https://doi.org/10.3390/rs14092039.

Erkeling, G., Hiesinger, H., Reiss, D., Hielscher, F.J., Ivanov, M.A., 2011. The stratigraphy of the Amenthes region, Mars: time limits for the formation of fluvial, volcanic and tectonic landforms. Icarus 215 (1), 128–152. https://doi.org/10.1016/j.icarus.2011.06.041.

Favalli, M., Karatson, D., Mazzarini, F., Pareschi, M.T., Boschi, E., 2009. Morphometry of scoria cones located on a volcano flank: a case study from Mt. Etna (Italy), based on high-resolution LiDAR data. J. Volcanol. Geotherm. Res. 186, 320–330. https://doi.org/10.1016/j.jvolgeores.2009.07.011.

Fernandez Romero, S., Morata Barrado, P., Rivero Rodriguez, M.A., Vazquez Yañez, G.A., De Diego Custodio, E., Michelena, M.D., 2021. Vector magnetometry using remotely piloted aircraft systems: an example of application for planetary exploration. Remote Sens. 13, 390. https://doi.org/10.3390/rs13030390.

Galindo, I., Vegas, J., Romero, C., Llorente, M., Martín-González, E., Rubio, J.C., Sánchez, N., 2019. Geoheritage inventory of the Lanzarote and Chinijo Islands UNESCO global Geopark. In: Lanzarote and Chinijo Islands Geopark: From Earth to Space, pp. 31–45.

Gao, J.W., Rong, Z.J., Klinger, L., Li, X.Z., Liu, D., Wei, Y., 2021. A spherical harmonic martian crustal magnetic field model combining data sets of MAVEN and MGS. Earth Space Sci. 8. https://doi.org/10.1029/2021EA001860 e2021EA001860.

García Cacho, L., Romero, C., 2000. Fenómenos hidromagmáticos en Lanzarote. In: Astiz, M., García, A. (Eds.), Curso Internacional de Volcanología y Geofísica Volcánica. Cabildo insular de Lanzarote, pp. 153–162.

Hasenaka, T., Carmichael, I.S.E., 1985. A compilation of location, size, and geomorphological parameters of volcanoes of the Michoacán-Guanajuato volcanic field, Central Mexico. Geofis. Int. 24-4, 577–607.

Hauber, E., Bleacher, J., Gwinner, K., Williams, D., Greeley, R., 2009. The topography and morphology of low shields and associated landforms of plains volcanism in the Tharsis region of Mars. J. Volcanol. Geotherm. Res 185 (1–2), 69–95.

Inbar, M., Risso, C., 2001. A morphological and morphometric analysis of a high density cinder cone volcanic field — Payun Matru, south-central Andes, Argentina. Zeitschrift fuer Geomorphologie 45 (3), 321–343.

Instituto Geográfico Nacional, 2015. MDT02-REGCAN95-HU28–1082-1-COB2.tif, Modelo Digital del Terreno – MDT02. Instituto Geográfico Nacional, Madrid, Spain. – present day. https://www.idee.es/csw-inspire-idee/srv/spa/catalog.search?**Ametadata*spaignMDT02_;Iy8v!!D9dNQwwGXtA!WUOSUkOmKIz-x2kFwQKnjDaU6wFks3b3q6waxc5LLT5EiVPNMMw2iuB9dDke7JP16xP8v0Q2jIxt8kb9QKyJv2i$.

Instituto Geográfico Nacional, 2023. PNOA_MA_OF_WGS84_HU28_h25_1082_1.tif, Ortofotos del Plan Nacional de Ortofotografía Aérea (PNOA) Máxima Actualidad de España. Instituto Geográfico Nacional, Madrid, Spain. https://www.idee.es/csw-inspire-idee/srv/spa/catalog.search?**Ametadata*spaignPNOAMA_;Iy8v!!D9dNQwwGXtA!WUOSUkOmKIz-x2kFwQKnjDaU6wFks3b3q6waxc5LLT5EiVPNMMw2iuB9dDke7JP16xP8v0Q2jIxt8kb9QLkdwGWf.

Kervyn, M., Ernst, G.G.J., Carracedo, J.C., Jacobs, P., 2012. Geomorphometric variability of "monogenetic" volcanic cones: evidence from Mauna Kea, Lanzarote and experimental cones. J. Geomorphol. 136, 59–75. https://doi.org/10.1016/j.geomorph.2011.04.009.

Keszthelyi, L.P., Jaeger, W., Dundas, C.M., Martínez-Alonso, S., McEwen, A.S., Milazzo, M.P., 2010. Hydrovolcanic features on Mars: Preliminary observations from the first Mars year of HiRISE imaging. Icarus 205, 211–229. https://doi.org/10.1016/j.icarus.2009.08.020.

Langlais, B., Thébault, E., Houliez, A., Purucker, M.E., Lillis, R.J., 2019. A new model of the crustal magnetic field of Mars using MGS and MAVEN. J. Geophys. Res.: Planets 124, 1542–1569. https://doi.org/10.1029/2018JE005854.

Lesur, V., Hamoudi, M., Choi, Y., et al., 2016. Building the second version of the World Digital magnetic Anomaly Map (WDMAM). Earth Planet Sp. 68, 27. https://doi.org/10.1186/s40623-016-0404-6.

Lillis, R.J., Robbins, S., Manga, M., Halekas, J.S., Frey, H.V., 2013. Time history of the martian dynamo from crater magnetic field analysis. J. Geophys. Res.: Planets 118 (7), 1488–1511. https://doi.org/10.1002/jgre.20105.

Lorenz, V., 1986. On the growth of maars and diatremes and its relevance to the formation of tuff rings. Bull. Volcanol. 48, 265–274.

Malin, M.C., 1977. Comparison of volcanic features of Elysium (Mars) and Tibesti (Earth). Geol. Soc. Am. Bull. 88 (7), 908–919. https://doi.org/10.1130/0016-7606(1977)88%3C908:COVFOE%3E2.0.CO;2.

Malin, M.C., Bell, J.F., Cantor, B.A., Caplinger, M.A., Calvin, W.M., Clancy, R.T., Edgett, K.S., Edwards, L., Haberle, R.M., James, P.B., Lee, S.W., Ravine, M.A., Thomas, P.C., Wolff, M.J., 2007. Context camera investigation on board the Mars reconnaissance orbiter. J. Geophys. Res. 112, E05S04. https://doi.org/10.1029/2006JE002808_;!!D9dNQwwGXtA!WUOSUkOmKIz-x2kFwQKnjDaU6wFks3b3q6waxc5LLT5EiVPNMMw2iuB9dDke7JP16xP8v0Q2jIxt8kb9QGfiwJXo.

Mateo, E., Martínez-Frías, J., Vegas, J., 2019. Lanzarote and Chinijo Islands Geopark: From Earth to Space. Springer. https://doi.org/10.1007/978-3-030-13130-2.

McGill, G.E., 1989. Buried topography of Utopia, Mars: persistence of a giant impact depression. J. Geophys. Res. Solid Earth 94 (B3), 2753–2759. https://doi.org/10.1029/JB094iB03p02753.

Mittelholz, A., Johnson, C.L., Morschhauser, A., 2018. A new magnetic field activity proxy for Mars from MAVEN data. J. Geophys. Res. Lett. 45, 5899–5907. https://doi.org/10.1029/2018GL078425.

Mittelholz, A., Johnson, C.L., Feinberg, J.M., Langlais, B., Phillips, R.J., 2020. Timing of the martian dynamo: New constraints for a core field 4.5 and 3.7 Ga ago. Sci. Adv. 6 (18), eaba0513. https://doi.org/10.1126/sciadv.aba0513.

Mittelholz, A., Heagy, L., Johnson, C.L., Bapst, J., Espley, J., Fraeman, A.A., Langlais, B., Lillis, R., Rapin, W., 2023. Exploring Martian magnetic fields with a Helicopter. Planet. Sci. J. 4 (8), 155. https://doi.org/10.3847/PSJ/ace9c1.

NASA, 2019. JPL-Caltech. https://mars.nasa.gov/resources/6471/driving-distances-on-mars-and-the-moon (accessed 22 February 2024).

Perez-Torrado, F.J., Carracedo, J.C., Rodriguez-Gonzalez, A., Rodríguez-Badiola, E., Paris, R., Troll, V.R., Wiesmaier, S., 2013. Eruptive styles at the Teide volcanic complex. In: Carracedo, J.C., Troll, V.R. (Eds.), Teide Volcano: Geology and Eruptions of a Highly Differentiated Oceanic Stratovolcano, pp. 213–231.

Pike, R.J., 1978. Volcanoes on the inner planets: some preliminary comparisons of gross topography. Proc. Lunar Sci. Conf. IX 3239–3273.

Plescia, J.B., 1990. Recent flood lavas in the Elysium region of Mars. Icarus 88 (2), 465–490. https://doi.org/10.1016/0019-1035(90)90095-Q.

Reitz, J.R., Milford, F.J., Christy, R.W., 2008. Foundations of Electromagnetic Theory, 4th edition. Addison-Wesley. ISBN: 978-0321581747.

Romero, C., Dóniz, J., García Cacho, L., Guillén, C., Coello, E., 2007. Nuevas evidencias acerca del origen hidromagmático del conjunto volcánico Caldera Blanca/Risco Quebrado (Lanzarote, Islas Canarias). Resúmenes XII Reunión Nacional de Cuaternario, Ávila.

Sandu, C., Kiefer, W.S., 2012. Degassing history of Mars and the lifespan of its magnetic dynamo. Geophys. Res. Lett. 39 (3). https://doi.org/10.1029/2011GL050225.

Settle, M., 1979. The structure and emplacement of cinder cone fields. Am. J. Sci. 279, 1089–1107.

Skinner Jr., J.A., Tanaka, K.L., 2007. Evidence for and implications of sedimentary diapirism and mud volcanism in the southern Utopia highland–lowland boundary plain. Mars. Icarus 186 (1), 41–59. https://doi.org/10.1016/j.icarus.2006.08.013.

Skinner Jr., J.A., Tanaka, K.L., Rodriguez, J.A.P., Kargel, J.S., 2005. The Southern utopia highland-lowland boundary: basin structural controls on aquifer development and volatile-driven resurfacing. In: 36th Annual Lunar and Planetary Science Conference, p. 2119.

Smith, D.E., Zuber, M.T., Frey, H.V., Garvin, J.B., Head, J.W., Muhleman, D.O., Pettengill, G.H., et al., 2001. Mars orbiter laser altimeter—experiment summary after the first year of global mapping of Mars. J. Geophys. Res. 106 (E10), 23689–23722. https://doi.org/10.1029/2000JE001364.

Smith, P.H., et al., 2009. H2O at the Phoenix landing site. Science 325, 58–61. https://doi.org/10.1126/science.1172339.

Sphengineering.com, 2025. UgCS - Drone Flight Planning Software. https://www.sphengineering.com/flight-planning/ugcs (accessed 22 February 2024).

Spohn, T., 2011. Heat Flow (Planetary). In: Gargaud, M. (Ed.), Encyclopedia of Astrobiology. Springer, Berlin, Heidelberg. https://doi.org/10.1007/978-3-642-11274-4_708.

Tada, N., Ichihara, H., Nakano, M., Utsugi, M., Koyama, T., Kuwatani, T., Baba, K., Maeno, F., Takagi, A., Takeo, M., 2021. Magnetization structure of Nishinoshima volcano, Ogasawara island arc, obtained from magnetic surveys using an unmanned aerial vehicle. J. Volcanol. Geotherm. Res. 419 (2021), 107349. https://doi.org/10.1016/j.jvolgeores.2021.107349.

Thébault, E., Finlay, C.C., Beggan, C.D., 2015. International geomagnetic reference field: the 12th generation. J. Earth Planets Sp. 67, 79. https://doi.org/10.1186/s40623-015-0228-9.

Vespermann, D., Scmincke, H., 2000. Scoria cones and tuff rings. In: Sigurdsson (Ed.), Encyclopedia of Volcanoes. AP, San Diego, pp. 683–694.

WASP™-200 LRF, 2025. Attollo Engineering. https://attolloengineering.com/product/wasp-200-lrf/ (accessed 22 February 2024).

White, J.D.L., Houghton, B., 2000. Surtseyan and Related Phreatomagmatic Eruptions. In: Sigurdsson (Ed.), Encyclopedia of Volcanoes. AP, San Diego, pp. 477–494.

Zheng, Y., Li, S., Xing, K., Zhang, X., 2021. Unmanned aerial vehicles for magnetic surveys: a review on platform selection and interference suppression. Drones 5, 93. https://doi.org/10.3390/drones5030093.